

A proposal for detecting weak electromagnetic waves around 2.6 μm wavelength with Sr optical clock

Ruo-Shui Han(韩弱水), Wei Wang(王伟), and Tao Wang(汪涛)

Citation: Chin. Phys. B, 2024, 33 (**4**): 043201. DOI: 10.1088/1674-1056/ad1b45
Journal homepage: http://cpb.iphy.ac.cn; http://iopscience.iop.org/cpb

What follows is a list of articles you may be interested in

New designed helical resonator to improve measurement accuracy of magic radio frequency

Tian Guo(郭天), Peiliang Liu(刘培亮), and Chaohong Lee(李朝红)
Chin. Phys. B, 2022, 31 (**9**): 093201. DOI: 10.1088/1674-1056/ac6944

Velocity-selective spectroscopy measurements of Rydberg fine structure states in a hot vapor cell

Jun He(何军), Dongliang Pei(裴栋梁), Jieying Wang(王杰英), Junmin Wang(王军民)
Chin. Phys. B, 2017, 26 (**11**): 113202. DOI: 10.1088/1674-1056/26/11/113202

Rubidium-beam microwave clock pumped by distributed feedback diode lasers

Chang Liu(刘畅), Sheng Zhou(周晟), Yan-Hui Wang(王延辉), Shi-Min Hou(侯士敏)
Chin. Phys. B, 2017, 26 (**11**): 113201. DOI: 10.1088/1674-1056/26/11/113201

Automatic compensation of magnetic field for a rubidium space cold atom clock

Lin Li(李琳), Jingwei Ji(吉经纬), Wei Ren(任伟), Xin Zhao(赵鑫), Xiangkai Peng(彭向凯), Jingfeng Xiang(项静峰), Desheng Lü(吕德胜), Liang Liu(刘亮)
Chin. Phys. B, 2016, 25 (**7**): 073201. DOI: 10.1088/1674-1056/25/7/073201

The ac Stark shifts of the terahertz clock transitions of barium

Yu Geng-Hua (余庚华), Geng Ying-Ge (耿鹰鸽), Li Long (李隆), Zhou Chao (周超), Duan Cheng-Bo (段丞博), Chai Rui-Peng (柴瑞鹏), Yang Yong-Ming (杨永明)
Chin. Phys. B, 2015, 24 (**10**): 103201. DOI: 10.1088/1674-1056/24/10/103201

A proposal for detecting weak electromagnetic waves around 2.6 μm wavelength with Sr optical clock

Ruo-Shui Han(韩弱水)[1,2], Wei Wang(王伟)[1,2,†], and Tao Wang(汪涛)[1,2,3,‡]

[1] *Department of Physics, and Chongqing Key Laboratory for Strongly Coupled Physics, Chongqing University, Chongqing* 401331, *China*
[2] *Center of Modern Physics, Institute for Smart City of Chongqing University in Liyang, Liyang* 213300, *China*
[3] *State Key Laboratory of Quantum Optics and Quantum Optics Devices, Shanxi University, Taiyuan* 030006, *China*

(Received 13 October 2023; revised manuscript received 29 December 2023; accepted manuscript online 5 January 2024)

Infrared signal detection is widely used in many fields. Due to the detection principle, however, the accuracy and range of detection are limited. Thanks to the ultra stability of the ^{87}Sr optical lattice clock, external infrared electromagnetic wave disturbances can be responded to. Utilizing the ac Stark shift of the clock transition, we propose a new method to detect infrared signals. According to our calculations, the theoretical detection accuracy in the vicinity of its resonance band of 2.6 μm can reach the order of 10^{-14} W, while the minimum detectable signal of common detectors is on the order of 10^{-10} W.

Keywords: infrared signal detection, ^{87}Sr optical lattice clock, ac Stark shift, ultra stability

PACS: 32.30.Bv, 42.50.Nn, 06.30.Ft **DOI:** 10.1088/1674-1056/ad1b45

1. Introduction

The infrared (IR) spectrum is characterized as the range extending from the boundary of visible red light (0.78 μm) to 1000 μm.[1] According to Planck's law of black-body radiation (BBR), objects with temperatures ranging from approximately 3 K to 3800 K all exhibit peak radiation wavelengths within the infrared spectrum, encompassing the majority of objects in the universe.[2] Therefore, whether employed on Earth or in space, IR detection technology provides great potential for various applications, including IR communication, imaging, remote sensing, and exploration.[3] Moreover, IR detection technology offers unique features, such as its ability to function in darkness compared to visible detectors, or its passive detection capabilities distinguishing itself from microwave detection technology.[4]

The advancement of IR detector technology is closely connected with semiconductor IR detectors, which belong to one class of photon detectors.[5] In these detectors, radiation is absorbed within the material through interaction with electrons, and the resulting electrical output signal is due to the altered electronic energy distribution. As a result, photon detectors exhibit a selective wavelength response per unit of incident radiation power. Another class of detectors is thermal detectors.[5] Such detectors operate by absorbing incident radiation to alter the materials' temperature, and the subsequent change in a physical property is used to generate an electrical output. The signals in thermal detectors do not rely on the photonic nature of the incident radiation, making them generally wavelength-independent but only depending on the radiant power.[4]

Among all physical quantities, time and frequency can be measured most accurately by humans, which is more than 5 orders of magnitude higher than other physical quantities. If the detection of infrared signals can be converted into the measurement of time or frequency, the detection accuracy may be greatly improved. As one of the most accurate time measurement instruments in the world, the fractional frequency instability and uncertainty of the best optical clocks based on neutral atoms[6–9] and single ions[10,11] have reached the unprecedented level of 10^{-18}, which can be employed to redefine the unit of the second of the international system of units. Optical lattice clocks (OLCs) can also be used in the field of other scientific research, such as fundamental constants variation measurement,[12–14] gravitational wave detection,[15] topological dark matter hunting,[16] and space research and applications.[17] In addition, OLCs have been investigated for global navigation satellite systems and geodetic applications.[18]

When building an optical clock platform, reseachers usually wish to reduce the interference of the external environment as much as possible,[19] because external disturbances will greatly affect the accuracy and stability of the optical clock. In other words, weak external signals can significantly affect the frequency of the optical lattice clock. There are many weak external disturbances in OLCs, among which the black-body radiation of the environment located in IR spectra, is dominant.[20,21] Therefore, using these features, the measurement of the IR signal can be converted into a measurement of time, and much higher detection accuracy can be achieved

†Corresponding author. E-mail: weiwangphys@163.com
‡Corresponding author. E-mail: tauwaang@cqu.edu.cn

© 2024 Chinese Physical Society and IOP Publishing Ltd

compared to the traditional infrared detection method. In this paper, starting from estimating the polarizabilities of the system, we calculate the frequency shift which can be observed accurately in experiments by OLCs. Then, according to the frequency shift, a scheme is proposed to infer the magnitude of the IR signal.

2. Theoretical basis

Black-body radiation, i.e., IR signal, is a major source of systematic uncertainty for numerous prominent lattice[20,21] and ion[22,23] clocks. Among all optical clocks currently developing, strontium (Sr) atoms exhibit the most significant frequency shift.[24] Such essential AC Stark shift is mainly caused by the electric field from the ambient heat in the laboratory and can be calculated as

$$\Delta\nu = \frac{-1}{2\varepsilon_0 ch}\int_0^\infty \Delta\alpha(\omega)\mathcal{I}(\omega)\,\mathrm{d}\omega, \tag{1}$$

where $\mathcal{I}(\omega)$ is the light intensity per angular frequency, and $\Delta\alpha(\omega)$ is the polarizability difference between two energy levels. In the ^{87}Sr OLC, the two internal states are $5s^2\,{}^1S_0$ with the polarizability $\alpha_s(\omega)$ and $5s5p\,{}^3P_0$ with $\alpha_p(\omega)$, respectively. Polarizability differences $\Delta\alpha(\omega) = \alpha_p(\omega) - \alpha_s(\omega)$. We consider a case in which the linewidth of the signal is very narrow, then Eq. (1) can be approximated as

$$\Delta\nu \approx \frac{-1}{2\varepsilon_0 ch}\Delta\alpha(\omega)\mathcal{I}(\omega)\Delta\omega. \tag{2}$$

Finally, IR signals are expressed as

$$\mathcal{I}(\omega) = \frac{-2\Delta\nu\cdot\varepsilon_0 ch}{\Delta\omega\Delta\alpha(\omega)}. \tag{3}$$

We note that the frequency shift can be measured accurately in the current ^{87}Sr OLC platform. Once the polarizabilities are known, the IR spectrum can be extrapolated well.

Now we turn to the formulas of two state polarizabilities,

$$\alpha_v(\omega) = \frac{2}{3(2J+1)}\sum_k \frac{\langle k|D|v\rangle^2(E_k - E_v)}{(E_k - E_v)^2 - \omega^2}, \tag{4}$$

where ω is the angular frequency of external radiation, v denotes the two clock states $^1S_0$ and $^3P_0$, k denotes other states, E_k, E_v and $\langle k|D|v\rangle$ are the corresponding energies and matrix elements, and D is the electric dipole moment. J is the total angular momentum, which is zero for the clock states. There are ten and four atomic states that have great influences on the states $^1S_0$ and $^3P_0$, respectively, as shown in Table 1. Substituting these states' energies and transition matrix elements into Eq. (4), the polarizabilities $\alpha_s(\omega)$ and $\alpha_p(\omega)$ are obtained as shown in Fig. 1. Here the polarizability is in atomic units, 1 a.u. of polarizability = 1.6488×10^{-41} C$^2\cdot$m$^2\cdot$J^{-1}. The polarizability of $5s5p\,{}^3P_0$ resonates at 2.6 μm (the blue dotted line), while that of $5s^2\,{}^1S_0$ is much less sensitive to the wavelength (the red solid line).

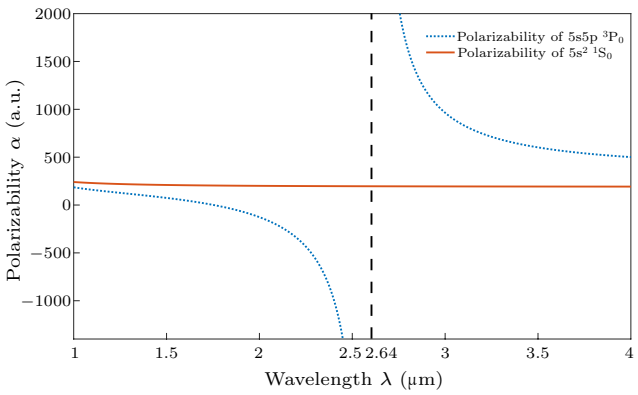


Fig. 1. Polarizabilities of $5s^2\,{}^1S_0$ and $5s5p\,{}^3P_0$ in the 1–4 μm band.

Table 1. List of the states, whose contributions reproduce the polarizabilities of two clock states. The corresponding energy differences and transition matrix elements are also given.

$5s5p\,{}^3P_0$			$5s^2\,{}^1S_0$		
State	Wavelength	Matrix elements D	State	Wavelength	Matrix elements D
$5s4d\,{}^3D_1$	2642.4	2.714	$5s5p\,{}^3P_1$	689.5	0.158
$5s6s\,{}^3S_1$	682.0	1.972	$5s5p\,{}^1P_1$	460.9	5.272
$5s5d\,{}^3D_1$	484.2	2.458	$5s6p\,{}^1P_1$	293.3	0.281
$5p^2\,{}^3P_1$	471.5	2.627	$4d5p\,{}^1P_1$	242.9	0.517
$5s7s\,{}^3S_1$	433.3	0.522			
$5s6d\,{}^3D_1$	394.3	1.175			
$5s8s\,{}^3S_1$	377.1	0.302			
$5s7d\,{}^3D_1$	361.4	0.822			
$5s9s\,{}^3S_1$	348.4	0.270			
$5s8d\,{}^3D_1$	336.7	0.820			

To verify the correctness of the above theory, we calculate the effect of black-body radiation at room temperature on ^{87}Sr OLC platform. The energy per unit angular frequency radiated vertically from a black body of temperature T per unit surface area per unit time is

$$\mathcal{I}(\omega, T) = \frac{\hbar}{4\pi^3 c^2}\frac{\omega^3}{\mathrm{e}^{\hbar\omega/k_\mathrm{B}T} - 1}. \tag{5}$$

We know that the intensity of black-body radiation on the atom

clouds is only related to the solid angle that the black body occupies around the atoms. Assuming the solid angle θ_0, the frequency shift of the clock transition is given by

$$\Delta\nu_{\mathrm{BBR}} = \frac{-\theta_0}{2\varepsilon_0 ch}\int_0^{\infty}\Delta\alpha(\omega)\mathcal{I}(\omega)\,\mathrm{d}\omega. \tag{6}$$

Using the data of Ref. [25] (the room temperature is 294.89 K), and the total solid angle is 0.16258π sr, the calculated frequency shift is -0.0171 Hz. Compared our result with that from Ref. [25], the error is less than 1%, which shows the validity of our theory.

3. Technical route

Now, we explain how to detect IR signals based on the OLC platform. The main idea is to probe the frequency of OLC before and after importing IR signals, from which the IR spectrum can be inferred.

3.1. Preparation of ^{87}Sr optical clock system

In experiments, the strontium atomic beam is emitted from a furnace heated to 500 °C with a velocity of 460 m/s. Using a Zeeman slower with ten coils, the velocity of the atomic beam is decreased from approximately 460 m/s to 50 m/s. The strontium atoms undergo further cooling and confinement within a two-stage magneto-optical trap (MOT). For the initial Doppler cooling stage, the dipole-permitted transition $5s^2\,{}^1S_0(F=9/2)$—$5s5p\,{}^1P_1(F=11/2)$ (with a 461 nm wavelength) is utilized; the associated cooling threshold is approximately in the sub-millikelvin domain. After the first-stage cooling, the atomic temperature remains significantly higher than the trap depth of the optical lattice, thus further cooling is required. The transition between the singlet and triplet states, termed the intercombination $5s^2\,{}^1S_0(F=9/2)$—$5s5p\,{}^3P_1(F=11/2)$ (with a 689 nm wavelength), is employed during the second Doppler cooling stage. This leads to a cooling limit approaching the sub-microkelvin domain. Following the two-step cooling and trapping process, a one-dimensional (1-D) horizontal optical lattice operating at 813 nm captures the cooled atoms within the Lamb–Dicke regime.[26] After the cold atoms are loaded into the optical lattice, the clock transition is excited by the clock laser to detect the transition rate. The transition $5s^2\,{}^1S_0$–$5s5p\,{}^3P_0$ at 698 nm serves as the clock transition due to its exceptionally narrow natural linewidth, approximately 1 mHz. After the clock laser is locked to the ultra-low-expansion cavity, the short-term stability of the output laser reaches the 10^{-15} level. However, its long-term stability and accuracy are poor. Therefore, the strontium atomic clock transition needs to be used as a frequency reference to achieve long-term stability for the clock laser, which is known as the closed-loop operation of the optical clock.[27] Such a clock experimental sequence ends by measuring the absolute frequency of the clock laser using a femtosecond optical frequency comb. For more details of the experimental process, please see Refs. [19,28–30].

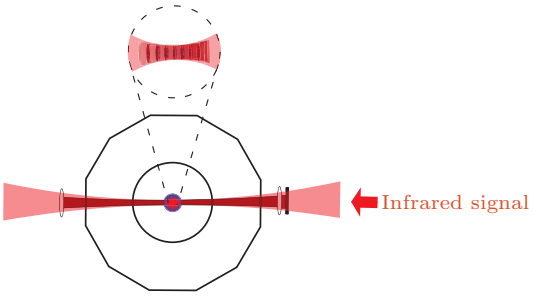


Fig. 2. Light path diagram of the process of signal detection.

3.2. Signal detection

During the preceding experimental process, we additionally input IR signal into the system, which should be first filtered out owing to the background noise. After that, we then introduce the signal into the Fabry–Pérot cavity optical filter to pick up a specific frequency range entering the OLC. Note that the center frequency and half-width of output signals can be adjusted with the help of the Fabry–Pérot cavity filter. The light path diagram of the whole process of signal detection is shown in Fig. 2, where three off-axis parabolic mirrors are needed to collimate the signal to match the size of the optical lattice. The processed electromagnetic signals may be likened unto Gaussian beams, wherein the waist radius equals that of the optical lattice. In the diagram, the dark red rays represent the lattice light, while the light red rays represent the incident infrared signal. It is evident that the waist radii of both are equal at their centers, but at the edges, the spot size of the infrared signal is larger than that of the lattice light. This is due to the incident signal being in the mid-infrared range, which has a wavelength longer than the lattice light's 813 nm. Approximately 86.5% of the total power is encompassed within the waist radius. However, since the spot size of the incident signal is larger than that of the lattice light at the edges, the actual power of the signal entering the optical lattice will be less than 86.5%. The spot size ratio of the 2.6 μm signal to the lattice light at the edge of the optical lattice is approximately 1.07, and this ratio varies with the wavelength of the signal. The actual signal received by the optical lattice needs to be calibrated experimentally. The schematic diagram of the optical lattice is shown within the dotted circle. Consequently, we focus the signal on the atoms as much as possible to increase the response of the system. The measurement is made through a time-division self-comparison method, which involves using an optical clock alternately as two optical clocks in different time periods. Before entering the optical clock, the signal

passes through a mechanical switch, which alters the state of light passage in different periods. In each cycle, the clock laser is locked to the atomic frequency through a closed-loop operation and the mechanical switch will alternate between the open and closed states. After integrating over some cycles, comparing the clock laser average frequencies of different cycles allows for the determination of the frequency offset caused by the signal.

4. Simulation and analysis

We consider the signal eventually captured by ^{87}Sr atoms as Lorentzian, whose power spectral density is given by

$$\mathcal{I}(\omega) = \frac{1}{\pi}\left[\frac{\gamma}{(\omega-\omega_0)^2+\gamma^2}\right]. \tag{7}$$

Here ω_0 is the center frequency of the spectrum with the magnitude of the order of 10^{14}, and γ is the spectral line width with the magnitude of 10^9. The Lorentzian line shape is normalized as

$$\int_0^\infty \frac{1}{\pi}\left[\frac{\gamma}{(\omega-\omega_0)^2+\gamma^2}\right] \mathrm{d}\omega = 1. \tag{8}$$

Substituting Eq. (7) into Eq. (1), we then obtain the frequency offset caused by the signal per W/m^2.

We now present our simulation results. The optical lattice in our system can be considered as a cylinder with a diameter of 40 μm and a height of 400 μm, as can be seen in Fig. 2, and the minimum projection is a circle with area $(20\ \mu\mathrm{m})^2 \times \pi \approx 1256.6\ \mu\mathrm{m}^2$. We set the waist radius to match the radius of the optical lattice. Within the waist radius approximately 86.5% of the total power is encompassed. If the signal with a total power of 1 W is focused on the optical lattice, the power sensed by the optical lattice will be 0.83 W and an intensity of 6.7×10^8 W/m^2 can be generated. According to these data, the frequency shift caused by each watt of signal in different bands can be calculated. The results for wavelengths in the range 1–4 μm are shown in Fig. 3. The signal bandwidths corresponding to Figs. 3(a), 3(b), 3(c), and 3(d) are 1 nm, 10 nm, 50 nm, and 100 nm, respectively. As shown in Fig. 3, the bandwidth can significantly affect the system's response. The narrower the bandwidth of the signal, the higher and sharper the peak of the system's response. Figure 3(a) shows a very narrow and high peak at 2.64 μm. As the bandwidth of the incident signal increases, the peak height of the system response decreases, and the width increases. Note that between the positive peak and negative peak, the system response decreases first and then increases, which means that there is a small interval around 2.64 μm in which the system gives little response. We will elaborate in detail on this phenomenon later. We stress that, based on our results, i.e., Fig. 3, one can immediately read the IR spectrum from the experimental standpoint; whereas the frequency shift is extracted by subtracting the measured transition frequency with applying the IR signal from that without it.

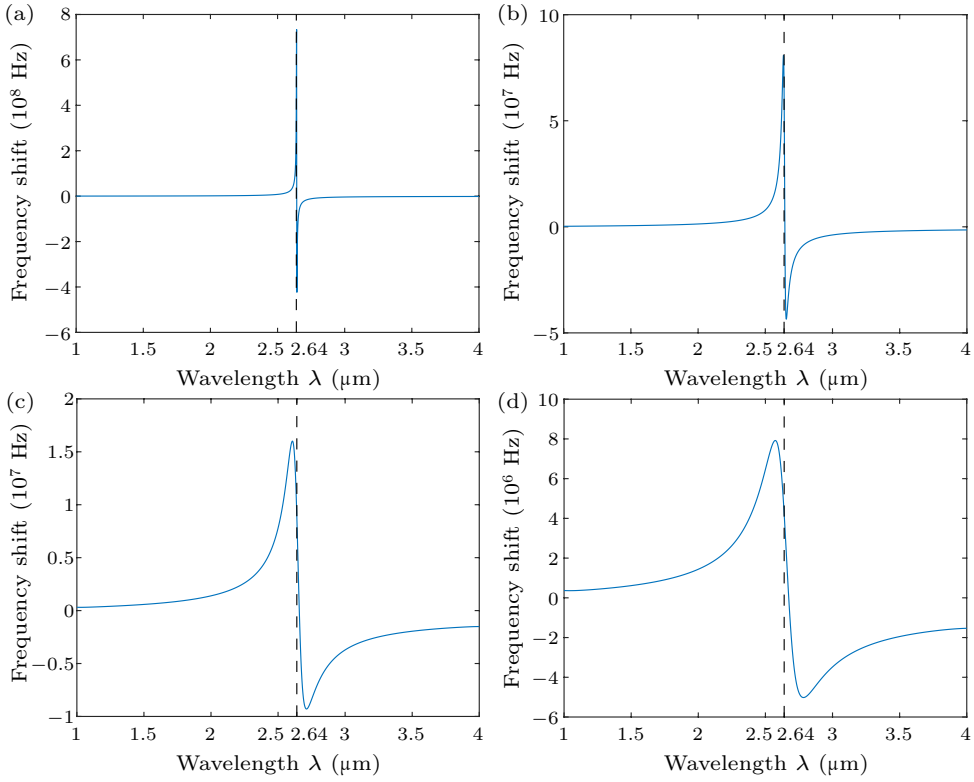


Fig. 3. Frequency shift per Watt of signal in wavelength range 1–4 μm with different signal bandwidth.

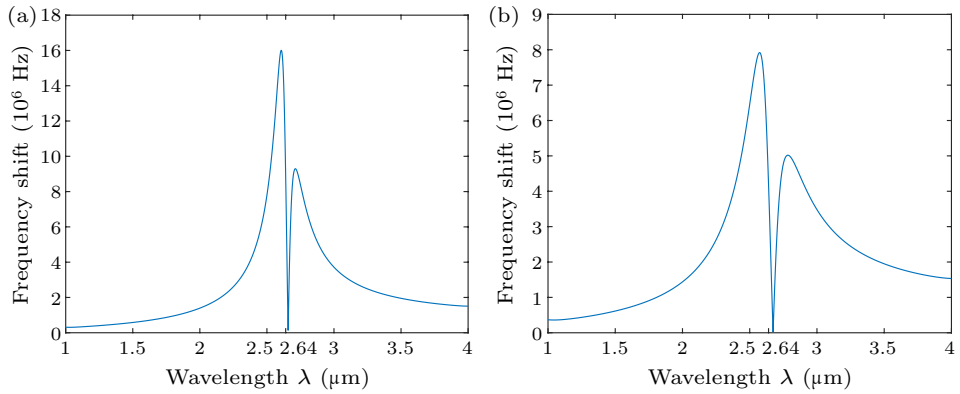


Fig. 4. Absolute value of frequency shift per Watt of signal in wavelength range 1–4 μm with different signal bandwidths.

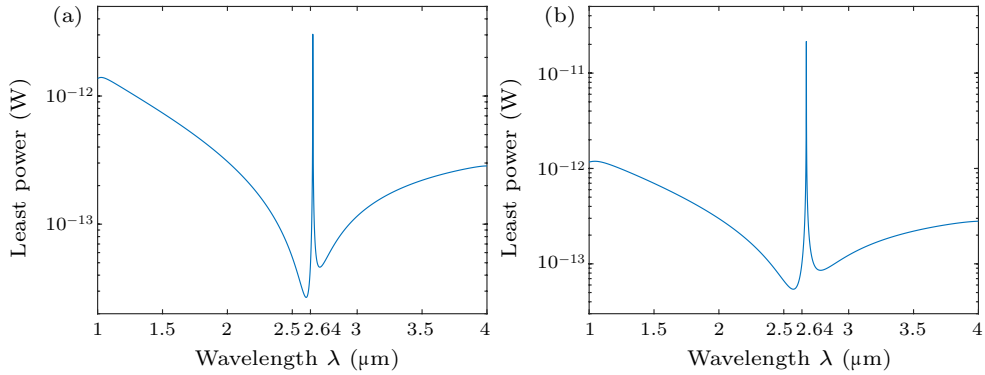


Fig. 5. Minimum detectable signal in wavelength range 1–4 μm with different signal bandwidths.

Table 2. Measurement accuracy of some typical detectors and OLC in the band of 2.6 μm.

Type of detectors	Minimum detectable signal (W)
InGaAs photodiode detectors	2.6×10^{-9}
Thermopile detectors	9×10^{-7}
InAs photovoltaic detectors	1.6×10^{-10}
InAsSb photovoltaic detectors	2.2×10^{-9}
InSb photovoltaic detectors	6.6×10^{-10}
Type-Ⅱ superlattice detectors	1.1×10^{-9}
Sr-87 optical lattice clock*	2.7×10^{-14}*

We now illustrate the detection capability by the absolute value of the frequency shift. Figure 4 shows the absolute value of frequency shift per watt of signal in wavelength range 1–4 μm with different signal bandwidths. We give two different signal bandwidths, 50 nm and 100 nm, which are relatively easy to achieve in practice. Figure 4(a) shows the result of 50 nm bandwidth, while Fig. 4(b) shows that of 100 nm bandwidth. It is clearly seen that in the 2.64 μm interval the system response first decreases and then increases. This interval is the blind area of the system. For 50 nm bandwidth the interval is approximately 100 nm, and for 100 nm bandwidth the interval is approximately 200 nm. This is because, when the signal is at the resonant wavelength (2.64 μm), half of the signal causes a positive frequency shift and the other half causes a negative one, which cancels each other out. Thus, the system has very high accuracy around 2.64 μm, while the accuracy drops when the signal is exactly at 2.64 μm.

To demonstrate the advantage of the present scheme, we next analyze measurement accuracy. From Figs. 3 and 4 one can see that the frequency shift has a very large response to the signal near the wavelength of 2.64 μm, and a very weak signal can be detected. Combined with theoretical stability of OLC of 10^{-21}, the theoretical limit of the detectable radiation intensity at the wavelength of 2.6 μm is estimated to be 2.7×10^{-14} W, while the detectable radiation intensity at the wavelength of 2.5 μm is estimated to be 5.3×10^{-14} W, with an incident signal with a bandwidth of 50 nm. It is worth explaining that the measurement only takes advantage of the stability of the optical clock. There are many systematic effects that affect the absolute frequency of optical lattice clock, such as collisional shift, Zeeman shift, and black-body radiation shift, but they have little impact on the measurement proposed in this study because this measurement is based on a time-division self-comparison method, which utilize the same system to eliminate those shifts. To compare the detection capability of the OLC system with others, we list several typical detectors that can detect IR signals in the wavelength of 2.6 μm in Table 2. It is clear that the method of this study, which is starred, is far better than other detectors on the market (can be improved by 4 orders of magnitude). In Fig. 5 we illustrate the minimum detectable signal. To highlight the magnitude of detection accuracy more prominently, we use a logarithmic scale on the vertical axis. Figures 5(a) and 5(b) cor-

respond to incident signal bandwidths of 50 nm and 100 nm, respectively. In the resonance region of both graphs, specifically at 2.64 μm, there is a noticeable decrease in detection accuracy. However, the minimum detectable signals around the resonance points have reached the order of 10^{-14} W, and the detection accuracy remains above 10^{-12} W across the entire detection wave spectrum. Providing common detectors of minimum detectable amplitudes of 10^{-10} W in that band, measurement accuracy of the present proposal have been improved at least in two order of magnitude.

5. Conclusion and outlook

In summary, we have proposed a new approach to detect weak infrared signals based on ^{87}Sr optical lattice clocks. The present scheme has been tested by re-evaluating the effect of black-body radiation and the error is less than one percent compared with the previous results in literature. Considering the ultra stability of the ^{87}Sr OLC, we have also estimated the measurement accuracy. The theoretical detection accuracy in the 1–4 μm band can reach the order of 10^{-12} W, while in the vicinity of its resonance band of 2.6 μm, it can be the order of 10^{-14} W. In 2022, a 'multiplexed' one-dimensional optical lattice clock has been implemented, in which spatially resolved strontium atom ensembles are trapped in the same optical lattice, interrogated simultaneously by a shared clock laser and read-out in parallel.[28] In that work, a relative statistical uncertainty of 8.9×10^{-20} was reached after 3.3 h of averaging. It is demonstrated that applications involving optical clock comparisons need not be limited by the instability of the local oscillator. According to this work, we anticipate that the actual smallest detectable signals would be on the order of 10^{-10} W in the 1–4 μm band, and on the order of 10^{-12} W in the resonance band of 2.6 μm.

Acknowledgment

Project supported by the National Natural Science Foundation of China (Grant No. 12274045).

References

[1] Rogalski A 2011 *Infrared detectors* 2nd edn. (Boca Raton: Taylor & Francis)
[2] Dautcour G and Wallis G 1968 *Fortschritte Der Physik* **16** 545
[3] Coates J P 1996 *Appl. Spectrosc. Rev.* **31** 179
[4] Rogalski A 2012 *Opto-Electron. Rev.* **20** 279
[5] Rogalski A 2002 *Infrared Phys. Technol.* **43** 187
[6] Bloom B J, Nicholson T L, Williams J R, Campbell S L, Bishof M, Zhang X, Zhang W, Bromley S L and Ye J 2014 *Nature* **506** 71
[7] Hinkley N, Sherman J A, Phillips N B, Schioppo M, Lemke N D, Beloy K, Pizzocaro M, Oates C W and Ludlow A D 2013 *Science* **341** 1215
[8] Nicholson T L, Campbell S L, Hutson R B, Marti G E, Bloom B J, McNally R L, Zhang W, Barrett M D, Safronova M S, Strouse G F, Tew W L and Ye J 2015 *Nat. Commun.* **6** 6896
[9] Ushijima I, Takamoto M, Das M, Ohkubo T and Katori H 2015 *Nat. Photon.* **9** 185
[10] Huntemann N, Sanner C, Lipphardt B, Tamm Chr and Peik E 2016 *Phys. Rev. Lett.* **116** 063001
[11] Chou C W, Hume D B, Koelemeij J C J, Wineland D J and Rosenband T 2010 *Phys. Rev. Lett.* **104** 070802
[12] Blatt S, Ludlow A D, Campbell G K, Thomsen J W, Zelevinsky T, Boyd M M, Ye J, Baillard X, Fouché M, Le Targat R, Brusch A, Lemonde P, Takamoto M, Hong F L, Katori H and Flambaum V V 2008 *Phys. Rev. Lett.* **100** 140801
[13] Godun R M, Nisbet-Jones P B R, Jones J M, King S A, Johnson L A M, Margolis H S, Szymaniec K, Lea S N, Bongs K and Gill P 2014 *Phys. Rev. Lett.* **113** 210801
[14] Huntemann N, Lipphardt B, Tamm Chr, Gerginov V, Weyers S and Peik E 2014 *Phys. Rev. Lett.* **113** 210802
[15] Kolkowitz S, Pikovski I, Langellier N, Lukin M D, Walsworth R L and Ye J 2016 *Phys. Rev. D* **94** 124043
[16] Derevianko A and Pospelov M 2014 *Nat. Phys.* **10** 933
[17] Ludlow A D, Boyd M M, Ye J, Peik E and Schmidt P O 2015 *Rev. Mod. Phys.* **87** 637
[18] Chou C W, Hume D B, Rosenband T and Wineland D J 2010 *Science* **329** 1630
[19] Wang Y B, Yin M J, Ren J, Xu Q F, Lu B Q, Han J X, Guo Y and Chang H 2018 *Chin. Phys. B* **27** 023701
[20] Targat R L, Lorini L, Coq Y L, Zawada M, Guéna J, Abgrall M, Gurov M, Rosenbusch P, Rovera D G, Nagórny B, Gartman R, Westergaard P G, Tobar M E, Lours M, Santarelli G, Clairon A, Bize S, Laurent P, Lemonde P and Lodewyck J 2013 *Nat. Commun.* **4** 2109
[21] Ludlow A D, Zelevinsky T, Campbell G K, Blatt S, Boyd M M, Miranda M H G de, Martin M J, Thomsen J W, Foreman S M, Ye J, Fortier T M, Stalnaker J E, Diddams S A, Coq Y L, Barber Z W, Poli N, Lemke N D, Beck K M and Oates C W 2008 *Science* **319** 5871
[22] Huntemann N, Okhapkin M, Lipphardt B, Weyers S, Tamm C and Peik E 2012 *Phys. Rev. Lett.* **108** 090801
[23] Madej A A, Dubé M, Zhou Z, Bernard J E and Gertsvolf M 2012 *Phys. Rev. Lett.* **109** 203002
[24] Safronova M S, Kozlov M G and Clark C W 2012 *IEEE Trans. Ultr. Ferr. Freq. Control* **59** 439
[25] Li T, Lu X T, Zhang Q, Kong D H, Wang Y B and Chang H 2019 *Acta Phys. Sin.* **68** 093701 (in Chinese)
[26] Blatt S, Thomsen J W, Campbell G K, Ludlow A D, Swallows M D, Martin M J, Boyd M M and Ye J 2009 *Phys. Rev. A* **80** 052703
[27] Lu X T, Guo F, Wang Y B, Xu Q F, Zhou C H, Xia J J, Wu W J and Chang H 2023 *Metrologia* **60** 015008
[28] Wang Y B, Lu X T, Lu B Q, Kong D H and Chang H 2018 *Appl. Sci.* **8** 2194
[29] Lu X T, Yin M J, Li T, Wang Y B and Chang H 2020 *Appl. Sci.* **10** 1440
[30] Bothwell T, Kedar D, Oelker E, Robinson J M, Bromley S L, Tew W L, Ye J and Kennedy C J 2019 *Metrologia* **56** 065004